THE JOURNAL OF PHYSICAL CHEMISTRY LETTERS
A JOURNAL OF THE AMERICAN CHEMICAL SOCIETY

pubs.acs.org/JPCL

Letter

Coexistence of Incoherent and Ultrafast Coherent Exciton Transport in a Two-Dimensional Superatomic Semiconductor

James M. Baxter, Christie S. Koay, Ding Xu, Shan-Wen Cheng, Jakhangirkhodja A. Tulyagankhodjaev, Petra Shih, Xavier Roy, and Milan Delor*

Cite This: *J. Phys. Chem. Lett.* 2023, 14, 10249−10256

Read Online

ACCESS | Metrics & More | Article Recommendations | Supporting Information

ABSTRACT: Fully leveraging the remarkable properties of low-dimensional semiconductors requires developing a deep understanding of how their structure and disorder affect the flow of electronic energy. Here, we study exciton transport in single crystals of the two-dimensional superatomic semiconductor $CsRe_6Se_8I_3$, which straddles a photophysically rich yet elusive intermediate electronic-coupling regime. Using femtosecond scattering microscopy to directly image exciton transport in $CsRe_6Se_8I_3$, we reveal the rare coexistence of coherent and incoherent exciton transport, leading to either persistent or transient electronic delocalization depending on temperature. Notably, coherent excitons exhibit ballistic transport at speeds approaching an extraordinary 1600 km/s over 300 fs. Such fast transport is mediated by J-aggregate-like superradiance, owing to the anisotropic structure and long-range order of $CsRe_6Se_8I_3$. Our results establish superatomic crystals as ideal platforms for studying the intermediate electronic-coupling regime in highly ordered environments, in this case displaying long-range electronic delocalization, ultrafast energy flow, and a tunable dual transport regime.

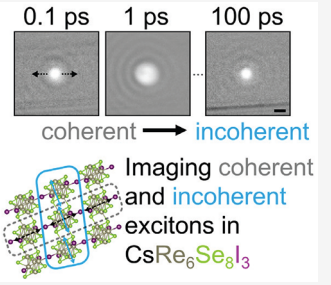

Atomically precise clusters[1−3] are unique superatomic building blocks for designing semiconductors with diverse electronic, magnetic, and chemical properties.[4−9] These superatoms can be synthetically and postsynthetically modified to introduce desired functionality, and linked into ordered networks, enabling control over the resulting collective properties with exquisite precision.[10−12] The realization of macroscopic single crystals of van der Waals (vdW) superatomic semiconductors that can be exfoliated to the two-dimensional (2D) limit provides an additional tuning knob for controlling electronic transport and light−matter interactions through dimensionality reduction,[13−15] providing a robust route to accelerate the development of new optoelectronic technologies.

A key objective of research in low-dimensional materials is to improve our understanding of the transport of excitons (coulomb-bound electron−hole pairs). Exciton transport is typically described in two limiting regimes: incoherent, thermally activated hopping associated with spatially localized (Frenkel-like) excitons, often observed in molecular semiconductors with weak electronic coupling or disorder-induced localization,[16−21] and coherent, band-like transport associated with delocalized (Wannier-like) excitons, typical of inorganic semiconductors, wherein transport is described as ballistic motion interrupted by scattering with phonons and impurities.[20−27] Superatomic semiconductors display electronic and structural features between those of molecular and inorganic semiconductors,[3,7,8] in a regime where the Bohr radii (∼1−2 nm) and binding energies (∼100 meV) of excitons are intermediate between Frenkel and Wannier pictures.[13] A similar deduction can be reached by noting that the magnitude of the exciton transfer integral is similar to site energy disorder (Supporting Information Section 1), placing superatomic crystals in the intermediate-coupling regime as defined in the molecular exciton literature.[28] This regime, often associated with macroscopically disordered systems such as photosynthetic organisms and polymer networks,[28−33] has proven a rich but still little-understood ground for complex exciton photophysics. 2D superatomic semiconductors, which we synthesize and exfoliate as macroscopic single-crystal flakes, represent some of the best-controlled systems to study this elusive electronic regime.

Here, we study exciton transport in $CsRe_6Se_8I_3$, a 2D superatomic semiconductor in which octahedral Re_6Se_8 clusters[34,35] are connected through intercluster Re−Se linkages along the *a*-axis and across Re−I−Re bridging ligands along the *c*-axis, creating 2D sheets with strong in-plane anisotropy (Figure 1a).[9] The sheets stack through vdW interactions along the *b*-axis and can be exfoliated (Figure 1b, Supporting Information Section 2). $CsRe_6Se_8I_3$ is structurally related to $Re_6Se_8Cl_2$,[7,13,36] which was recently found to exhibit superconductivity[36] and record-breaking exciton mean free paths.[37]

Received: August 15, 2023
Revised: November 2, 2023
Accepted: November 3, 2023
Published: November 8, 2023

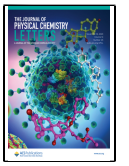

https://doi.org/10.1021/acs.jpclett.3c02286
J. Phys. Chem. Lett. 2023, 14, 10249−10256

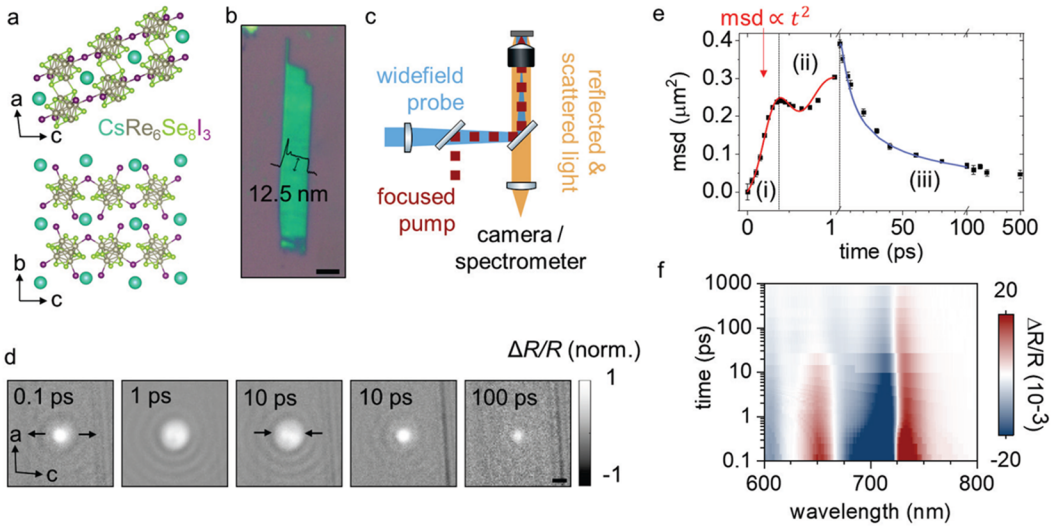

Figure 1. Exciton transport in $CsRe_6Se_8I_3$ at 5 K. (a) Crystal structure of $CsRe_6Se_8I_3$. (b) Optical microscopy image of a 12.5 nm thick $CsRe_6Se_8I_3$ crystal (the height profile measured by atomic force microscopy is overlaid). The scale bar is 5 μm. (c) StroboSCAT microscope: The pump pulse is focused on the sample. At controllable time delays after the pump, reflected and scattered light from a widefield probe pulse are imaged on a camera or imaging spectrometer. More details are given in Supporting Information Section 2. (d) StroboSCAT time series at 5 K obtained with 515 nm pump and 730 nm probe. Each image is plotted on a normalized contrast scale. The scale bar is 1 μm. (e) Mean squared displacement (msd) extracted from data in panel d. i, ii, and iii refer to the three transport regimes discussed in the text. The red line is from a numerical model describing a ballistic-to-diffusive transition of the initially coherent exciton. The blue line is from a numerical model combining a fast, short-lived species with a slow, long-lived species (see text for details). Error bars are one standard deviation. (f) Transient reflectance spectra obtained with 515 nm pump and probing with polarization perpendicular to the *a*-axis at 5 K.

The added complexity of asymmetric bonding in $CsRe_6Se_8I_3$ introduces strongly polarized light−matter interactions.[9] By directly imaging exciton transport in $CsRe_6Se_8I_3$, we reveal coherent, ballistic exciton transport within the first picosecond, followed by antidiffusion and slower, thermally activated transport. Temperature-dependent analysis of this transport behavior and its anisotropy reveals that this exotic behavior stems from a mixture of localized and coherently delocalized excitons in $CsRe_6Se_8I_3$. Remarkably, long-range coherent exciton transport is maintained up to 200 K, promoted by the unique, rigid J-aggregate-like structure of $CsRe_6Se_8I_3$, suggesting a new design rule to drastically enhance electronic energy flow in low-dimensional semiconductors.

To directly image exciton propagation in $CsRe_6Se_8I_3$, we leverage the few-nanometer spatial sensitivity and femtosecond temporal resolution of stroboscopic scattering microscopy (stroboSCAT, Figure 1c and Supporting Information Section 2),[22,38,39] a nonlinear version of interferometric scattering microscopy.[40,41] A ∼100 fs, above-gap diffraction-limited pump generates bound excitons. At controllable time delays, a wide-field probe with a central wavelength of 730 nm, close to the exciton resonance, images the sample with and without the pump pulse in a backscattering geometry. The pump-induced change in the reflected light intensity, $\Delta R/R$, reports on the spatiotemporal evolution of excitons. Figure 1d shows a representative stroboSCAT data set on a 12.5 nm thick $CsRe_6Se_8I_3$ flake (Figure 1b) taken at 5 K. The positive signal due to photoinduced bleaching of the lowest-energy transition represents the spatial distribution of the pump-induced exciton population. Close to time-zero, an exciton distribution with a Gaussian width of $\sigma(0\ \text{ps}) = 285$ nm is obtained, close to the expected time-zero profile of 242 nm according to the pump−probe spatial cross-correlation (Figure S1). By 1 ps, this distribution has expanded to $\sigma(1\ \text{ps}) = 786$ nm, indicating a rapid exciton migration away from the excitation spot. This expansion is followed by an unusual apparent contraction of the spatial profile from 2 to 100 ps.

To quantitatively analyze exciton transport, we extract the mean squared displacement $\text{msd} = \sigma^2(t) - \sigma^2(0)$, where $\sigma^2(t)$ is the variance of the spatial distribution extracted from the average of a 2D Gaussian fit to each stroboSCAT image (Supporting Information Section 3). The msd can be modeled as $\text{msd} = 2Dt^{\alpha}$, where D is the diffusivity. For normal (Fickian) diffusion, we expect $\alpha = 1$. $\alpha = 2$ is associated with ballistic transport, and subdiffusive transport exhibits $0 < \alpha < 1$ or more complex behavior.[22,38,42−44] Figure 1e displays the msd from 0 to 500 ps. Three distinct transport regimes are observed, which we discuss below sequentially: (i) ultrafast ballistic expansion over the first 300 fs; (ii) a short contraction period in the range 400−650 fs followed by normal diffusion up to 1 ps; and (iii) apparent negative diffusion up to 500 ps.

In transport regime i, the population profile expands ∼0.24 μm^2 within 300 fs, corresponding to a migration length of 480 nm at an extraordinary velocity of 1600 km/s. The msd over the first 300 fs is ballistic ($\alpha = 2$, Figure S2), suggesting wavelike (coherent, scatter-free) expansion of the exciton population. Even on subpicosecond time scales, the clear observation of wavelike energy transport in ultrafast microscopy is rare. Related time-resolved observations of ballistic transport thus far are typically in materials excited far-from-equilibrium[45] and in polaritonic systems.[46−50] In our results, the msd depends weakly on pump energy and fluence, showing ultrafast expansion even upon band-edge excitation (Figures S3 and S4), indicating that the observed transport is unlikely to be affected by hot carrier effects,[45,51] thermal gradients[52] or phonon winds.[53,54] Furthermore, the results are reproducible in a range of flake thicknesses (from 12 to 250 nm) and is thus not related to self-hybridized polaritons.[50,55] We therefore deduce that ballistic transport in the first 300 fs is mediated by

https://doi.org/10.1021/acs.jpclett.3c02286
J. Phys. Chem. Lett. 2023, 14, 10249−10256

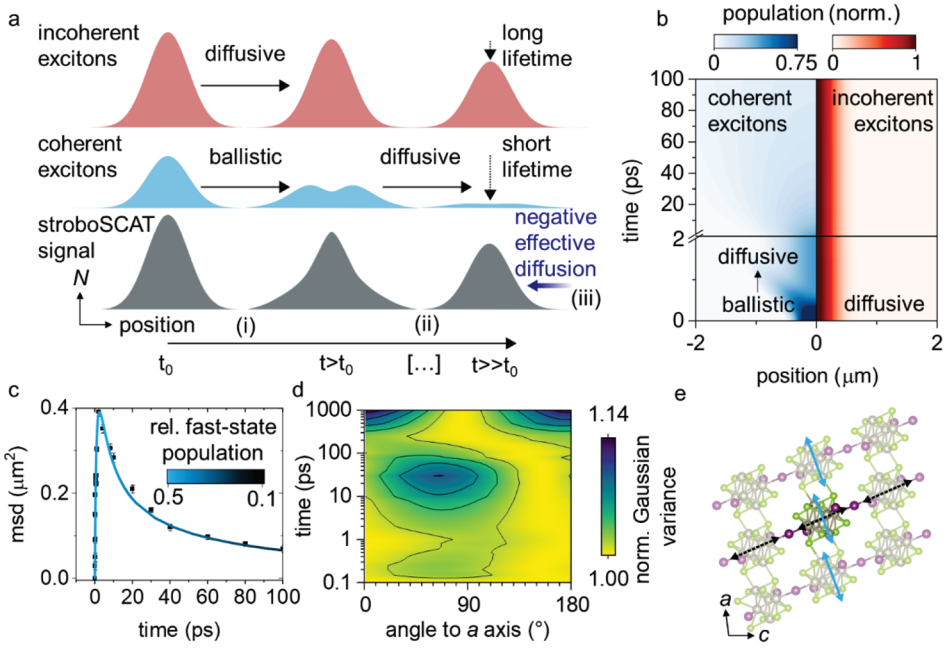

Figure 2. Exciton delocalization and anisotropy in $CsRe_6Se_8I_3$. (a) Evolution of population (N) profiles used to model negative effective diffusion. The stroboSCAT signal combines contributions from slow-moving and long-lived excitons undergoing diffusive transport (red) and fast-moving but short-lived excitons undergoing a ballistic-to-diffusive transition (blue). The sections labeled i, ii, and iii refer to the regimes discussed in the text and labeled in Figure 1e. (b) Evolution of the coherent and incoherent exciton populations as a function of space and time. (c) Fit of the two-state numerical model (solid line) to the exciton transport msd at 5 K. The line coloration indicates the relative population contribution of the fast-moving state. Error bars are one standard deviation. (d) Anisotropy of the stroboSCAT signal at 5 K: normalized Gaussian variance plotted as a function of angle from the a-axis. At early times, transport is enhanced along an angle ~70° from the a-axis. At later times, the population profile preferentially expands approximately parallel to the a-axis. (e) Projection of the transition dipoles for the two lowest (black dashed) and third lowest (blue) transitions.[9]

coherent delocalization of the exciton wave function, discussed in more detail below.

In transport regime ii, the population profile slightly contracts between 400 and 650 fs, followed by an expansion recovery until 2 ps (Figure 1e). A short contraction period was also observed for hot carriers in transition metal dichalcogenides[56] and excitons in quantum wells.[57,58] The latter case was explained by a loss of coherence associated with the first exciton−acoustic phonon scattering event. In line with this interpretation, we model our data using a ballistic → diffusive transition over an ensemble of photoexcitations (Supporting Information Section 4). Our model closely reproduces the experimental msd (red line in Figure 1e, detail in Figure S2). The transition at ~300 fs can thus be assigned to a phenomenological scattering or decoherence time of the initially coherent exciton population.[57]

In transport regime iii, the population appears to contract on itself over 500 ps, indicating negative effective diffusion. This intriguing effect has been observed and predicted in a variety of systems including 2D materials[59−61] and molecular crystals[62] and is explained by competing spatio-kinetic effects when multiple photoexcited species are present. Transient reflectance spectra of $CsRe_6Se_8I_3$ (Figure 1f), which displays a dominant response due to photoinduced bleaching of the lowest optical transition, support the notion that several species or competing processes are present: three components with subtly different spectral contributions and lifetimes of ~0.3, 11, and 440 ps are required to model the spectral evolution via global analysis (Figure S5). Similar to recent studies,[59] we model the observed antidiffusion using numerical simulations of a population mixture combining two distinct excitonic species (Figure 2a and Supporting Information Section 4). One species corresponds to the coherent excitons discussed above that are responsible for transport regimes i and ii, which propagate rapidly and are short-lived (blue in Figure 2a). The second species is a slow-propagating, diffusive species that is long-lived (red in Figure 2a). The model thus combines two distinct populations that are excited by the pump pulse in parallel and evolve independently from one another (Figures 2b). This model closely reproduces the overall msd extracted from stroboSCAT (Figure 2c). Thus, the apparent anti-diffusion of transport regime iii likely stems from the presence of at least two species evolving independently over different spatiotemporal scales, both contributing to the overall exciton transport behavior in $CsRe_6Se_8I_3$. We speculate that the two species correspond to momentum-direct (bright) and momentum-indirect (dark) excitons, as proposed in Handa et al.,[9] though further work is needed to confirm these assignments.

To understand the nature of the slow- and fast-moving species, we now turn to distinguishing their behavior by analyzing their degree of transport anisotropy and their temperature dependence. Given the anisotropic bonding in the ac plane of $CsRe_6Se_8I_3$, we expect corresponding anisotropy in exciton transport. Close inspection of the stroboSCAT data in Figure 1d reveals a subtle spatial asymmetry during the fast expansion and slow contraction stages. To quantitatively extract this anisotropy, Figure 2d plots the normalized Gaussian variance $\frac{\sigma^2(\theta,t)}{\sigma^2(\theta_{min},t)} / \frac{\sigma^2(\theta,0)}{\sigma^2_{min}(\theta_{min},0)}$, where θ

https://doi.org/10.1021/acs.jpclett.3c02286
J. Phys. Chem. Lett. 2023, 14, 10249−10256

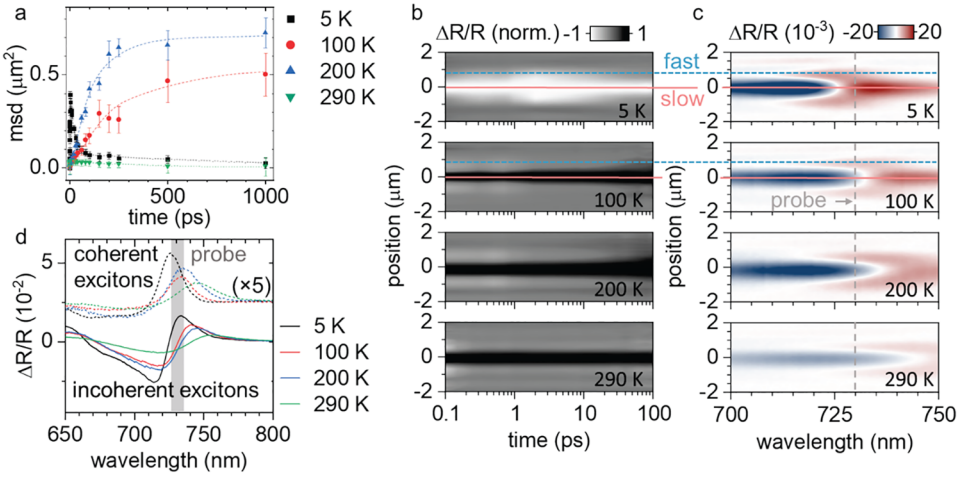

Figure 3. Temperature dependence of exciton transport in $CsRe_6Se_8I_3$. (a) Msd's extracted from stroboSCAT data at temperatures spanning 5 to 290 K (Figure S7). Dashed lines are to guide the eye. Error bars are one standard deviation. (b) Cross section of stroboSCAT signal with 515 nm excitation and 730 nm probe, measured at temperatures spanning 5 to 290 K. Contrast is normalized at each time delay to emphasize spatial spreading over time. (c) Spacetime transient reflectance (STR) spectra at 1 ps pump−probe time delay, measured at temperatures spanning 5 to 290 K. Horizontal lines across panels b and c emphasize that incoherent species (which remain around the pump excitation region at 0 μm) have slightly different spectral signatures than fast-moving species (which propagate ∼1 μm beyond the pump region within a picosecond). (d) Spectra at 0 ± 0.25 μm (labeled incoherent excitons) and at 1 ± 0.25 μm (labeled coherent excitons, offset for clarity) from the pump excitation spot at 1 ps pump−probe time delay, measured at temperatures spanning 5 to 290 K. The stroboSCAT probe wavelength used for data in panel b is indicated with the vertical gray lines in panels c and d.

is the angle from the crystal *a*-axis and θ_{min} is the angle along which the smallest width is observed in the 2D Gaussian distribution. During the period of fast expansion and negative diffusion, i.e., in the range 0−100 ps, the normalized Gaussian variance is largest around $\theta \approx 70°$, suggesting that exciton expansion of the short-lived species occurs primarily along this direction. Between 200 and 1000 ps, the dominant axis switches to $\theta \approx 5°$ from the *a*-axis and remains there until full population decay. These results indicate that the fast, short-lived excitons and the slow, long-lived excitons adopt different preferential transport axes.

To relate the observed anisotropy to the electronic structure of $CsRe_6Se_8I_3$, we compare our results against time-dependent density function theory (TD-DFT) calculations reported in Handa et al.,[9] which were shown to accurately capture the temperature-dependent polarized absorption and photoluminescence properties of the material. Calculations show that the transition dipoles for the two degenerate lowest-energy direct transition are oriented at an angle of ∼70° with respect to the *a*-axis (black dashed arrows in Figure 2e), identical with the experimentally inferred preferential transport direction of fast-propagating excitons. The approximately head-to-tail arrangement of these transition dipoles are reminiscent of J-aggregates.[9,20,63−65] Molecular J-aggregates are widely associated with microscopic superradiance,[66,67] wherein the dipoles at individual sites oscillate in-phase and constructively add to form a delocalized state with large transition dipole moment and short radiative lifetimes.[68−72] This delocalization correspondingly gives rise to enhanced, coherent exciton transport,[73−77] particularly in low-disorder systems. The anisotropic, ultrafast exciton expansion we observe in the first picosecond in $CsRe_6Se_8I_3$ is consistent with such J-type coherent delocalization of the excitonic wave function. Additional indicators reported in Figure S6 such as the anisotropy of the oscillator strength and temperature-dependent peak shifts are all consistent with our assignment of the lowest-energy direct transition to a J-aggregate-like state exhibiting microscopic superradiance.[9,20,63−65]

At later times (t > 100 ps, Figure 2d), once the fast excitons have decayed and only the slow species are left, we observe a preferential transport axis aligned approximately along the *a*-axis of $CsRe_6Se_8I_3$. This orientation is consistent with the calculated transition dipole orientation of the third-lowest direct transition[9] (blue arrows in Figure 2e). The apparent slow-moving nature of these excitons at 5 K suggests that they are fairly localized (Frenkel-like) incoherent excitons.

To support our assignment of coexisting coherent and incoherent excitons in $CsRe_6Se_8I_3$, we perform temperature-dependent stroboSCAT measurements. The msd's at 5, 100, 200, and 290 K are shown in Figure 3a. Corresponding stroboSCAT images from which msd's are extracted are shown in Figure S7, and population profile cross sections as a function of time are shown in Figure 3b. The data exhibit dramatic differences above 100 K compared to 5 K. First, the contrast in Figure 3b changes from a positive signal at 5 K to a primarily negative signal above 100 K. This change occurs because the optical gap red-shifts at higher temperatures, and the stroboSCAT probe wavelength switches from primarily preresonant to above-gap (Figure S6). Second, Figure 3b shows that the dominating dark contrast at a temperature higher than 5 K maintains a relatively narrow spatial distribution in the first 100 ps, suggesting this contrast is associated with the slower-moving species. Nevertheless, at 100 and 200 K, the dark contrast is surrounded by a bright "halo" at early times, suggesting that some excitons with a slightly different optical resonance have rapidly expanded; we explore this spectral dependence in more detail below. The spatial width of the bright halo at 1 ps decreases slightly with increasing temperature. We assign this bright contrast to the same coherently expanding excitons as those observed at 5 K, suggesting that some degree of exciton delocalization is

https://doi.org/10.1021/acs.jpclett.3c02286
J. Phys. Chem. Lett. 2023, 14, 10249−10256

maintained even in the presence of dynamic disorder at temperatures up to 200 K.

The msd's for the slow excitons at 5, 100, and 200 K exhibit increased diffusion lengths with increasing temperature (Figure 3a), characteristic of thermally activated (incoherent) transport, supporting our hypothesis of a dual transport regime in $CsRe_6Se_8I_3$. Although subdiffusive fits (i.e., msd = $2Dt^{\alpha}$ where $0 < \alpha < 1$) cannot describe the observed msd (Figure S8), we can estimate an effective diffusivity $D_{eff} = \mathrm{msd}(\tau)/2\tau$ over 1 ns of 2.5 cm^2/s at 100 K and 3.65 cm^2/s at 200 K, with even higher diffusivities at early times (Figure S8). These diffusivities are remarkably high for thermally activated exciton transport, which is typically limited to much less than 1 cm^2/s.[16,18,22,78] A plausible mechanism for the excellent transport properties of incoherent excitons in $CsRe_6Se_8I_3$ is transient exciton delocalization, whereby weakly localized excitons temporarily access delocalized states through thermal fluctuations. This process enables Frenkel-type excitons in intermediate-coupling systems to reach diffusivities exceeding 1 cm^2/s.[33,79−82] Energetic and long-range structural order are both considered crucial prerequisites to enable such transient delocalization.[79] The extended crystalline framework, low static disorder, and intermediate regime of excitons in $CsRe_6Se_8I_3$ make the latter an ideal candidate to observe and study this intriguing transport regime.

Surprisingly, stroboSCAT data at 290 K show an almost completely static distribution (Figures 3a,b and S8): neither coherent nor thermally activated transport is evident. This observation is also likely to be consistent with transient delocalization. The temperature dependence of exciton transport in the transient delocalization regime remains unstudied,[79] but likely exhibits a nonmonotonous trend: thermal fluctuations are required to access delocalized states, but excess disorder at high temperatures may entirely prevent delocalization, resulting in reduced diffusivities. In this scenario, the temperature trend of exciton diffusivities would exhibit a bell shape, similar to our observations.

As aforementioned, stroboSCAT data at 730 nm probe wavelength exhibits both bright and dark contrast depending on temperature, suggesting a switch from preresonant to above-gap probing as the optical gap redshifts with increasing temperature. To understand the effect of spectral shifts on stroboSCAT, and to tease out the different spectral contributions of the slow and fast species across different temperatures, we performed Spacetime Transient Reflectance (STR) microscopy (Supporting Information Section 2). STR is analogous to performing stroboSCAT experiments at many different probe wavelengths, albeit with lower signal-to-noise-ratio. We recently introduced this method[37] to enable directly correlating the transport properties of different energy carriers to their transient spectra. Figure 3c displays STR data from 5 to 290 K at a 1 ps pump−probe time delay; the y-axis is the spatial coordinate (with the pump centered at 0 μm), and the x-axis spectrally disperses the transient reflectance signal. Simultaneous spatial and spectral resolution allows distinguishing the coherent and incoherent species: At 1 ps pump−probe delay, only the coherent excitons have migrated beyond the diffraction-limited excitation region, whereas incoherent excitons are stationary over this time scale. The spectral weight and propagation distance of coherent excitons decrease with increasing temperature, consistent with stroboSCAT data. The horizontal lines stretching across Figure 3b,c emphasize that the coherent excitons (propagating to the blue dashed line in 1 ps) possess slightly different spectra compared with the incoherent excitons near 0 μm. This spectral dependence explains the bright "halo" at elevated temperatures in Figure 3b; for example, at 100 K, the stroboSCAT probe (vertical dashed line in Figure 3c) is preresonant with the coherent species resulting in bright contrast (positive $\Delta R/R$), but on-resonance with the incoherent species resulting in dark contrast (negative $\Delta R/R$). Therefore, STR allows independent tracking of the evolution of different species. These results confirm that the temperature dependence of the msd's in Figure 3a are not due to stroboSCAT preferentially probing different species due to spectral shifts; instead, the trend in msd's are driven by a progressive loss of coherent delocalization and to radically different incoherent exciton transport as temperature is raised.

Figure 3d extracts the transient spectra from STR at 1 ps of the incoherent (stationary) vs coherent (moving) species by plotting spectral line-cuts at 0 μm vs 1 μm away, respectively, from the excitation spot. The coherent excitons exhibit a peak ∼15−25 meV blueshifted from the incoherent excitons. Assuming this spectral difference approximately translates to an equivalent difference in the exciton state energies, we speculate that localized, incoherent excitons can transiently access the coherently delocalized state at temperatures >100 K (∼9 meV) through thermal fluctuations, enabling high average diffusivities on long time scales. At 5 K (∼0.4 meV), localized excitons are not able to access the delocalized states; incoherent and coherent excitons in this case evolve independently, explaining the fast expansion at early times followed by apparent negative diffusion, as discussed above. Overall, these results provide a concrete framework to explain both persistent (at 5 K) and transient (at 100−200 K) exciton delocalization in $CsRe_6Se_8I_3$ and illustrate the power of combining energy- and temperature-dependent spatiotemporally resolved microscopy for disentangling the complex transport dynamics of multicomponent excitonic systems.

Overall, we have observed the coexistence of coherent, delocalized excitons exhibiting ballistic transport and incoherent, localized excitons exhibiting thermally activated transport in the 2D superatomic semiconductor $CsRe_6Se_8I_3$. The coherent excitons, mediated by wave function delocalization through J-aggregate-like microscopic superradiance, propagate over half a micron ballistically (i.e., with no scattering losses) at ∼1600 km/s at 5 K and survive up to at least 200 K. Although coherent exciton delocalization in molecular J-aggregates has been the subject of intense study for its potential to mediate long-range energy transport, the direct observation of ballistic exciton transport mediated by this process is, to our knowledge, unprecedented. Furthermore, we demonstrate that, although incoherent species in $CsRe_6Se_8I_3$ exhibit the characteristic thermally activated transport properties of localized excitons, their very high diffusivities exceeding 1 cm^2/s suggest a novel transport regime such as transient delocalization, likely facilitated by the inherent long-range order and rigidity of our single-crystal superatomic framework. Our study thus establishes 2D superatomic semiconductors as an ideal platform to study the rich intermediate electronic-coupling regime including complex transport dynamics mediated by superradiance and transient delocalization. Future material designs will seek to enhance coherent exciton delocalization and energy transport through incorporation of anisotropic superatoms in asymmetric bonding frameworks

https://doi.org/10.1021/acs.jpclett.3c02286
J. Phys. Chem. Lett. 2023, 14, 10249−10256

favoring one-dimensional head-to-tail alignment of transition dipoles.

■ ASSOCIATED CONTENT

Supporting Information

The Supporting Information is available free of charge at https://pubs.acs.org/doi/10.1021/acs.jpclett.3c02286.

Sample and experimental details (Supporting Information Sections 1−3), simulation parameters (Supporting Information Section 4), and additional data including fluence- and pump-energy dependence in Figures S1−S8 (PDF)

■ AUTHOR INFORMATION

Corresponding Author

Milan Delor − *Department of Chemistry, Columbia University, New York, New York 10027, United States;* orcid.org/0000-0002-9480-9235; Email: milan.delor@columbia.edu

Authors

James M. Baxter − *Department of Chemistry, Columbia University, New York, New York 10027, United States;* orcid.org/0000-0002-4641-6760

Christie S. Koay − *Department of Chemistry, Columbia University, New York, New York 10027, United States*

Ding Xu − *Department of Chemistry, Columbia University, New York, New York 10027, United States*

Shan-Wen Cheng − *Department of Chemistry, Columbia University, New York, New York 10027, United States*

Jakhangirkhodja A. Tulyagankhodjaev − *Department of Chemistry, Columbia University, New York, New York 10027, United States*

Petra Shih − *Department of Chemistry, Columbia University, New York, New York 10027, United States;* orcid.org/0000-0002-6071-1803

Xavier Roy − *Department of Chemistry, Columbia University, New York, New York 10027, United States;* orcid.org/0000-0002-8850-0725

Complete contact information is available at: https://pubs.acs.org/10.1021/acs.jpclett.3c02286

Notes

The authors declare no competing financial interest.

■ ACKNOWLEDGMENTS

We thank Prof. Timothy Berkelbach and Dr. Taketo Handa (Columbia) for helpful discussions. This material is primarily based upon work supported by the National Science Foundation (NSF) through the Columbia MRSEC on Precision-Assembled Quantum Materials (PAQM) (DMR-2011738) and by the Air Force Office of Scientific Research (AFOSR) under grant number FA9550-22-1-0389 (M.D., X.R.). stroboSCAT instrument development was supported by the NSF under grant number DMR-2115625 (M.D.). Synthesis of the crystals was supported by the NSF CAREER award DMR-1751949 (X.R.). M.D. acknowledges support from the Arnold and Mabel Beckman Foundation through a Beckman Young Investigator award. J.A.T. was supported by the NSF Graduate Research Fellowship.

■ REFERENCES

(1) Chevrel, R.; Sergent, M.; Prigent, J. Sur de Nouvelles Phases Sulfurées Ternaires Du Molybdène. *J. Solid State Chem.* **1971**, *3*, 515−519.

(2) Long, J. R.; McCarty, L. S.; Holm, R. H. A Solid-State Route to Molecular Clusters: Access to the Solution Chemistry of $[Re_6Q_8]^{2+}$ (Q = S, Se) Core-Containing Clusters via Dimensional Reduction. *J. Am. Chem. Soc.* **1996**, *118*, 4603−4616.

(3) Khanna, S. N.; Jena, P. Atomic Clusters: Building Blocks for a Class of Solids. *Phys. Rev. B* **1995**, *51*, 13705−13716.

(4) Zhong, X.; Lee, K.; Meggiolaro, D.; Dismukes, A. H.; Choi, B.; Wang, F.; Nuckolls, C.; Paley, D. W.; Batail, P.; De Angelis, F.; Roy, X.; Zhu, X. Mo 6 S 3 Br 6 : An Anisotropic 2D Superatomic Semiconductor. *Adv. Funct. Mater.* **2019**, *29*, No. 1902951.

(5) Bartholomew, A. K.; Meirzadeh, E.; Stone, I. B.; Koay, C. S.; Nuckolls, C.; Steigerwald, M. L.; Crowther, A. C.; Roy, X. Superatom Regiochemistry Dictates the Assembly and Surface Reactivity of a Two-Dimensional Material. *J. Am. Chem. Soc.* **2022**, *144*, 1119−1124.

(6) Roy, X.; Lee, C.-H.; Crowther, A. C.; Schenck, C. L.; Besara, T.; Lalancette, R. A.; Siegrist, T.; Stephens, P. W.; Brus, L. E.; Kim, P.; Steigerwald, M. L.; Nuckolls, C. Nanoscale Atoms in Solid-State Chemistry. *Science* **2013**, *341*, 157−160.

(7) Lee, K.; Maehrlein, S. F.; Zhong, X.; Meggiolaro, D.; Russell, J. C.; Reed, D. A.; Choi, B.; De Angelis, F.; Roy, X.; Zhu, X. Hierarchical Coherent Phonons in a Superatomic Semiconductor. *Adv. Mater.* **2019**, *31*, No. 1903209.

(8) Li, Q.; Liu, F.; Russell, J. C.; Roy, X.; Zhu, X. Strong Polaronic Effect in a Superatomic Two-Dimensional Semiconductor. *J. Chem. Phys.* **2020**, *152*, No. 171101.

(9) Handa, T.; Shih, P.; Koay, C. S.; Nuckolls, C.; Roy, X.; Berkelbach, T. C.; Zhu, X. Anisotropically Fused Clusters Form a 2D Superatomic Sheet Exhibiting Polarized Light Emission. *J. Phys. Chem. C* **2023**, *127*, 1519−1526.

(10) Doud, E. A.; Voevodin, A.; Hochuli, T. J.; Champsaur, A. M.; Nuckolls, C.; Roy, X. Superatoms in Materials Science. *Nat. Rev. Mater.* **2020**, *5*, 371−387.

(11) He, S.; Okuno, S.; Ng, F. W.; Pang, X.; Esposito, D. V.; Orchanian, N. M.; Steigerwald, M. L.; Roy, X.; Nuckolls, C. Functional Monolayers on a Superatomic Pegboard. *J. Am. Chem. Soc.* **2023**, *145*, 8314−8318.

(12) He, S.; Evans, A. M.; Meirzadeh, E.; Han, S. Y.; Russell, J. C.; Wiscons, R. A.; Bartholomew, A. K.; Reed, D. A.; Zangiabadi, A.; Steigerwald, M. L.; Nuckolls, C.; Roy, X. Site-Selective Surface Modification of 2D Superatomic Re_6Se_8. *J. Am. Chem. Soc.* **2022**, *144*, 74−79.

(13) Zhong, X.; Lee, K.; Choi, B.; Meggiolaro, D.; Liu, F.; Nuckolls, C.; Pasupathy, A.; De Angelis, F.; Batail, P.; Roy, X.; Zhu, X. Superatomic Two-Dimensional Semiconductor. *Nano Lett.* **2018**, *18*, 1483−1488.

(14) Meirzadeh, E.; Evans, A. M.; Rezaee, M.; Milich, M.; Dionne, C. J.; Darlington, T. P.; Bao, S. T.; Bartholomew, A. K.; Handa, T.; Rizzo, D. J.; Wiscons, R. A.; Reza, M.; Zangiabadi, A.; Fardian-Melamed, N.; Crowther, A. C.; Schuck, P. J.; Basov, D. N.; Zhu, X.; Giri, A.; Hopkins, P. E.; Kim, P.; Steigerwald, M. L.; Yang, J.; Nuckolls, C.; Roy, X. A Few-Layer Covalent Network of Fullerenes. *Nature* **2023**, *613*, 71−76.

(15) Pinkard, A.; Champsaur, A. M.; Roy, X. Molecular Clusters: Nanoscale Building Blocks for Solid-State Materials. *Acc. Chem. Res.* **2018**, *51*, 919−929.

(16) Scholes, G. D. Long-Range Resonance Energy Transfer in Molecular Systems. *Annu. Rev. Phys. Chem.* **2003**, *54*, 57−87.

(17) Menke, S. M.; Holmes, R. J. Exciton Diffusion in Organic Photovoltaic Cells. *Energy Environ. Sci.* **2014**, *7*, 499−512.

(18) Mikhnenko, O. V.; Blom, P. W. M.; Nguyen, T.-Q. Exciton Diffusion in Organic Semiconductors. *Energy Environ. Sci.* **2015**, *8*, 1867−1888.

(19) Schröter, M.; Ivanov, S. D.; Schulze, J.; Polyutov, S. P.; Yan, Y.; Pullerits, T.; Kühn, O. Exciton−Vibrational Coupling in the

Dynamics and Spectroscopy of Frenkel Excitons in Molecular Aggregates. *Phys. Rep.* **2015**, *567*, 1−78.
(20) Hestand, N. J.; Spano, F. C. Expanded Theory of H- and J-Molecular Aggregates: The Effects of Vibronic Coupling and Intermolecular Charge Transfer. *Chem. Rev.* **2018**, *118*, 7069−7163.
(21) Bardeen, C. J. The Structure and Dynamics of Molecular Excitons. *Annu. Rev. Phys. Chem.* **2014**, *65*, 127−148.
(22) Ginsberg, N. S.; Tisdale, W. A. Spatially Resolved Photogenerated Exciton and Charge Transport in Emerging Semiconductors. *Annu. Rev. Phys. Chem.* **2020**, *71*, 1−30.
(23) Wang, L.; Beljonne, D. Flexible Surface Hopping Approach to Model the Crossover from Hopping to Band-like Transport in Organic Crystals. *J. Phys. Chem. Lett.* **2013**, *4*, 1888−1894.
(24) Shuai, Z.; Geng, H.; Xu, W.; Liao, Y.; André, J. M. From Charge Transport Parameters to Charge Mobility in Organic Semiconductors through Multiscale Simulation. *Chem. Soc. Rev.* **2014**, *43*, 2662−2679.
(25) Yang, F.; Cheng, S.; Zhang, X.; Ren, X.; Li, R.; Dong, H.; Hu, W. 2D Organic Materials for Optoelectronic Applications. *Adv. Mater.* **2018**, *30*, No. 1702415.
(26) Bässler, H.; Köhler, A. Charge Transport in Organic Semiconductors. In *Unimolecular and Supramolecular Electronics I. Topics in Current Chemistry*; Metzger, R., Ed.; Springer, 2011; Vol. *312*, pp 1−65.
(27) Troisi, A. Charge Transport in High Mobility Molecular Semiconductors: Classical Models and New Theories. *Chem. Soc. Rev.* **2011**, *40*, 2347−2358.
(28) Chenu, A.; Scholes, G. D. Coherence in Energy Transfer and Photosynthesis. *Annu. Rev. Phys. Chem.* **2015**, *66*, 69−96.
(29) Aragó, J.; Troisi, A. Regimes of Exciton Transport in Molecular Crystals in the Presence of Dynamic Disorder. *Adv. Funct. Mater.* **2016**, *26*, 2316−2325.
(30) Scholes, G. D.; Fleming, G. R.; Chen, L. X.; Aspuru-Guzik, A.; Buchleitner, A.; Coker, D. F.; Engel, G. S.; van Grondelle, R.; Ishizaki, A.; Jonas, D. M.; Lundeen, J. S.; McCusker, J. K.; Mukamel, S.; Ogilvie, J. P.; Olaya-Castro, A.; Ratner, M. A.; Spano, F. C.; Whaley, K. B.; Zhu, X. Using Coherence to Enhance Function in Chemical and Biophysical Systems. *Nature* **2017**, *543*, 647−656.
(31) Collini, E.; Scholes, G. D. Coherent Intrachain Energy Migration in a Conjugated Polymer at Room Temperature. *Science* **2009**, *323*, 369−373.
(32) Brédas, J.-L.; Sargent, E. H.; Scholes, G. D. Photovoltaic Concepts Inspired by Coherence Effects in Photosynthetic Systems. *Nat. Mater.* **2017**, *16*, 35−44.
(33) Sneyd, A. J.; Fukui, T.; Paleček, D.; Prodhan, S.; Wagner, I.; Zhang, Y.; Sung, J.; Collins, S. M.; Slater, T. J. A.; Andaji-Garmaroudi, Z.; MacFarlane, L. R.; Garcia-Hernandez, J. D.; Wang, L.; Whittell, G. R.; Hodgkiss, J. M.; Chen, K.; Beljonne, D.; Manners, I.; Friend, R. H.; Rao, A. Efficient Energy Transport in an Organic Semiconductor Mediated by Transient Exciton Delocalization. *Sci. Adv.* **2021**, *7*, No. eabh4232.
(34) Gray, T. G.; Rudzinski, C. M.; Meyer, E. E.; Holm, R. H.; Nocera, D. G. Spectroscopic and Photophysical Properties of Hexanuclear Rhenium(III) Chalcogenide Clusters. *J. Am. Chem. Soc.* **2003**, *125*, 4755−4770.
(35) Gabriel, J. C. P.; Boubekeur, K.; Uriel, S.; Batail, P. Chemistry of Hexanuclear Rhenium Chalcohalide Clusters. *Chem. Rev.* **2001**, *101*, 2037−2066.
(36) Telford, E. J.; Russell, J. C.; Swann, J. R.; Fowler, B.; Wang, X.; Lee, K.; Zangiabadi, A.; Watanabe, K.; Taniguchi, T.; Nuckolls, C.; Batail, P.; Zhu, X.; Malen, J. A.; Dean, C. R.; Roy, X. Doping-Induced Superconductivity in the van Der Waals Superatomic Crystal $Re_6Se_8Cl_2$. *Nano Lett.* **2020**, *20*, 1718−1724.
(37) Tulyagankhodjaev, J. A.; Shih, P.; Yu, J.; Russell, J. C.; Chica, D. G.; Reynoso, M. E.; Su, H.; Stenor, A. C.; Roy, X.; Berkelbach, T. C.; Delor, M. Room Temperature Wavelike Exciton Transport in a van Der Waals Superatomic Semiconductor. *Science* **2023**, *382*, 438−442.
(38) Zhu, T.; Snaider, J. M.; Yuan, L.; Huang, L. Ultrafast Dynamic Microscopy of Carrier and Exciton Transport. *Annu. Rev. Phys. Chem.* **2019**, *70*, 219−244.
(39) Delor, M.; Weaver, H. L.; Yu, Q.; Ginsberg, N. S. Imaging Material Functionality through Three-Dimensional Nanoscale Tracking of Energy Flow. *Nat. Mater.* **2020**, *19*, 56−62.
(40) Taylor, R. W.; Sandoghdar, V. Interferometric Scattering Microscopy: Seeing Single Nanoparticles and Molecules via Rayleigh Scattering. *Nano Lett.* **2019**, *19*, 4827−4835.
(41) Young, G.; Kukura, P. Interferometric Scattering Microscopy. *Annu. Rev. Phys. Chem.* **2019**, *70*, 301−322.
(42) Akselrod, G. M.; Deotare, P. B.; Thompson, N. J.; Lee, J.; Tisdale, W. A.; Baldo, M. A.; Menon, V. M.; Bulović, V. Visualization of Exciton Transport in Ordered and Disordered Molecular Solids. *Nat. Commun.* **2014**, *5*, 3646.
(43) Seitz, M.; Magdaleno, A. J.; Alcázar-Cano, N.; Meléndez, M.; Lubbers, T. J.; Walraven, S. W.; Pakdel, S.; Prada, E.; Delgado-Buscalioni, R.; Prins, F. Exciton Diffusion in Two-Dimensional Metal-Halide Perovskites. *Nat. Commun.* **2020**, *11*, 2035.
(44) Delor, M.; Slavney, A. H.; Wolf, N. R.; Filip, M. R.; Neaton, J. B.; Karunadasa, H. I.; Ginsberg, N. S. Carrier Diffusion Lengths Exceeding 1 Mm Despite Trap-Limited Transport in Halide Double Perovskites. *ACS Energy Lett.* **2020**, *5*, 1337−1345.
(45) Sung, J.; Schnedermann, C.; Ni, L.; Sadhanala, A.; Chen, R. Y. S.; Cho, C.; Priest, L.; Lim, J. M.; Kim, H. K.; Monserrat, B.; Kukura, P.; Rao, A. Long-Range Ballistic Propagation of Carriers in Methylammonium Lead Iodide Perovskite Thin Films. *Nat. Phys.* **2020**, *16*, 171−176.
(46) Freixanet, T.; Sermage, B.; Tiberj, A.; Planel, R. In-Plane Propagation of Excitonic Cavity Polaritons. *Phys. Rev. B* **2000**, *61*, 7233−7236.
(47) Xu, D.; Mandal, A.; Baxter, J. M.; Cheng, S.-W.; Lee, I.; Su, H.; Liu, S.; Reichman, D. R.; Delor, M. Ultrafast Imaging of Polariton Propagation and Interactions. *Nat. Commun.* **2023**, *14*, 3881.
(48) Balasubrahmaniyam, M.; Simkhovich, A.; Golombek, A.; Sandik, G.; Ankonina, G.; Schwartz, T. From Enhanced Diffusion to Ultrafast Ballistic Motion of Hybrid Light−Matter Excitations. *Nat. Mater.* **2023**, *22*, 338−344.
(49) Pandya, R.; Ashoka, A.; Georgiou, K.; Sung, J.; Jayaprakash, R.; Renken, S.; Gai, L.; Shen, Z.; Rao, A.; Musser, A. J. Tuning the Coherent Propagation of Organic Exciton-Polaritons through Dark State Delocalization. *Adv. Sci.* **2022**, *9*, No. 2105569.
(50) Pandya, R.; Chen, R. Y. S.; Gu, Q.; Sung, J.; Schnedermann, C.; Ojambati, O. S.; Chikkaraddy, R.; Gorman, J.; Jacucci, G.; Onelli, O. D.; Willhammar, T.; Johnstone, D. N.; Collins, S. M.; Midgley, P. A.; Auras, F.; Baikie, T.; Jayaprakash, R.; Mathevet, F.; Soucek, R.; Du, M.; Alvertis, A. M.; Ashoka, A.; Vignolini, S.; Lidzey, D. G.; Baumberg, J. J.; Friend, R. H.; Barisien, T.; Legrand, L.; Chin, A. W.; Yuen-Zhou, J.; Saikin, S. K.; Kukura, P.; Musser, A. J.; Rao, A. Microcavity-like Exciton-Polaritons Can Be the Primary Photoexcitation in Bare Organic Semiconductors. *Nat. Commun.* **2021**, *12*, 6519.
(51) Guo, Z.; Wan, Y.; Yang, M.; Snaider, J.; Zhu, K.; Huang, L. Long-Range Hot-Carrier Transport in Hybrid Perovskites Visualized by Ultrafast Microscopy. *Science* **2017**, *356*, 59−62.
(52) Perea-Causín, R.; Brem, S.; Rosati, R.; Jago, R.; Kulig, M.; Ziegler, J. D.; Zipfel, J.; Chernikov, A.; Malic, E. Exciton Propagation and Halo Formation in Two-Dimensional Materials. *Nano Lett.* **2019**, *19*, 7317−7323.
(53) Smith, L. M.; Preston, J. S.; Wolfe, J. P.; Wake, D. R.; Klem, J.; Henderson, T.; Morkoç, H. Phonon-Wind-Driven Transport of Photoexcited Carriers in a Semiconductor Quantum Well. *Phys. Rev. B* **1989**, *39*, 1862−1870.
(54) Glazov, M. M. Phonon Wind and Drag of Excitons in Monolayer Semiconductors. *Phys. Rev. B* **2019**, *100*, 45426.
(55) Munkhbat, B.; Baranov, D. G.; Stührenberg, M.; Wersäll, M.; Bisht, A.; Shegai, T. Self-Hybridized Exciton-Polaritons in Multilayers of Transition Metal Dichalcogenides for Efficient Light Absorption. *ACS Photonics* **2019**, *6*, 139−147.

https://doi.org/10.1021/acs.jpclett.3c02286
J. Phys. Chem. Lett. 2023, 14, 10249−10256

(56) Liu, Q.; Wei, K.; Tang, Y.; Xu, Z.; Cheng, X.; Jiang, T. Visualizing Hot-Carrier Expansion and Cascaded Transport in WS_2 by Ultrafast Transient Absorption Microscopy. *Adv. Sci.* **2022**, *9*, No. 2105746.
(57) Zhao, H.; Dal Don, B.; Schwartz, G.; Kalt, H. Ultrafast Breathinglike Oscillation in the Exciton Density of ZnSe Quantum Wells. *Phys. Rev. Lett.* **2005**, *94*, No. 137402.
(58) Zhao, H.; Dal Don, B.; Moehl, S.; Kalt, H.; Ohkawa, K.; Hommel, D. Spatiotemporal Dynamics of Quantum-Well Excitons. *Phys. Rev. B* **2003**, *67*, No. 035306.
(59) Rosati, R.; Perea-Causín, R.; Brem, S.; Malic, E. Negative Effective Excitonic Diffusion in Monolayer Transition Metal Dichalcogenides. *Nanoscale* **2020**, *12*, 356−363.
(60) Zhou, Y.-K.; Li, X.-Z.; Zhou, Q.-N.; Xing, R.-H.; Zhang, Y.; Bai, B.; Fang, H.-H.; Sun, H.-B. Transient Superdiffusion of Energetic Carriers in Transition Metal Dichalcogenides Visualized by Ultrafast Pump-Probe Microscopy. *Ultrafast Sci.* **2022**, *2022*, 0002.
(61) Ziegler, J. D.; Zipfel, J.; Meisinger, B.; Menahem, M.; Zhu, X.; Taniguchi, T.; Watanabe, K.; Yaffe, O.; Egger, D. A.; Chernikov, A. Fast and Anomalous Exciton Diffusion in Two-Dimensional Hybrid Perovskites. *Nano Lett.* **2020**, *20*, 6674−6681.
(62) Berghuis, A. M.; Raziman, T. V.; Halpin, A.; Wang, S.; Curto, A. G.; Rivas, J. G. Effective Negative Diffusion of Singlet Excitons in Organic Semiconductors. *J. Phys. Chem. Lett.* **2021**, *12*, 1360−1366.
(63) Chuang, C.; Bennett, D. I. G.; Caram, J. R.; Aspuru-Guzik, A.; Bawendi, M. G.; Cao, J. Generalized Kasha's Model: T-Dependent Spectroscopy Reveals Short-Range Structures of 2D Excitonic Systems. *Chem.* **2019**, *5*, 3135−3150.
(64) Deshmukh, A. P.; Geue, N.; Bradbury, N. C.; Atallah, T. L.; Chuang, C.; Pengshung, M.; Cao, J.; Sletten, E. M.; Neuhauser, D.; Caram, J. R. Bridging the Gap between H- and J-Aggregates: Classification and Supramolecular Tunability for Excitonic Band Structures in Two-Dimensional Molecular Aggregates. *Chem. Phys. Rev.* **2022**, *3*, No. 021401.
(65) Deshmukh, A. P.; Koppel, D.; Chuang, C.; Cadena, D. M.; Cao, J.; Caram, J. R. Design Principles for Two-Dimensional Molecular Aggregates Using Kasha's Model: Tunable Photophysics in Near and Short-Wave Infrared. *J. Phys. Chem. C* **2019**, *123*, 18702−18710.
(66) Fidder, H.; Knoester, J.; Wiersma, D. A. Superradiant Emission and Optical Dephasing in J-Aggregates. *Chem. Phys. Lett.* **1990**, *171*, 529−536.
(67) Spano, F. C.; Mukamel, S. Superradiance in Molecular Aggregates. *J. Chem. Phys.* **1989**, *91*, 683−700.
(68) De Boer, S.; Wiersma, D. A. Dephasing-Induced Damping of Superradiant Emission in J-Aggregates. *Chem. Phys. Lett.* **1990**, *165*, 45−53.
(69) Spano, F. C.; Kuklinski, J. R.; Mukamel, S. Cooperative Radiative Dynamics in Molecular Aggregates. *J. Chem. Phys.* **1991**, *94*, 7534−7544.
(70) Potma, E. O.; Wiersma, D. A. Exciton Superradiance in Aggregates: The Effect of Disorder, Higher Order Exciton-Phonon Coupling and Dimensionality. *J. Chem. Phys.* **1998**, *108*, 4894−4903.
(71) Arias, D. H.; Stone, K. W.; Vlaming, S. M.; Walker, B. J.; Bawendi, M. G.; Silbey, R. J.; Bulović, V.; Nelson, K. A. Thermally-Limited Exciton Delocalization in Superradiant Molecular Aggregates. *J. Phys. Chem. B* **2013**, *117*, 4553−4559.
(72) Doria, S.; Sinclair, T. S.; Klein, N. D.; Bennett, D. I. G.; Chuang, C.; Freyria, F. S.; Steiner, C. P.; Foggi, P.; Nelson, K. A.; Cao, J.; Aspuru-Guzik, A.; Lloyd, S.; Caram, J. R.; Bawendi, M. G. Photochemical Control of Exciton Superradiance in Light-Harvesting Nanotubes. *ACS Nano* **2018**, *12*, 4556−4564.
(73) Sharma, A.; Zhang, L.; Tollerud, J. O.; Dong, M.; Zhu, Y.; Halbich, R.; Vogl, T.; Liang, K.; Nguyen, H. T.; Wang, F.; Sanwlani, S.; Earl, S. K.; Macdonald, D.; Lam, P. K.; Davis, J. A.; Lu, Y. Supertransport of Excitons in Atomically Thin Organic Semiconductors at the 2D Quantum Limit. *Light Sci. Appl.* **2020**, *9*, 116.
(74) Abasto, D. F.; Mohseni, M.; Lloyd, S.; Zanardi, P. Exciton Diffusion Length in Complex Quantum Systems: The Effects of Disorder and Environmental Fluctuations on Symmetry-Enhanced Supertransfer. *Philos. Trans. R. Soc. A Math. Phys. Eng. Sci.* **2012**, *370*, 3750−3770.
(75) Caram, J. R.; Doria, S.; Eisele, D. M.; Freyria, F. S.; Sinclair, T. S.; Rebentrost, P.; Lloyd, S.; Bawendi, M. G. Room-Temperature Micron-Scale Exciton Migration in a Stabilized Emissive Molecular Aggregate. *Nano Lett.* **2016**, *16*, 6808−6815.
(76) Clark, K. A.; Krueger, E. L.; Vanden Bout, D. A. Direct Measurement of Energy Migration in Supramolecular Carbocyanine Dye Nanotubes. *J. Phys. Chem. Lett.* **2014**, *5*, 2274−2282.
(77) Haedler, A. T.; Kreger, K.; Issac, A.; Wittmann, B.; Kivala, M.; Hammer, N.; Köhler, J.; Schmidt, H.-W.; Hildner, R. Long-Range Energy Transport in Single Supramolecular Nanofibres at Room Temperature. *Nature* **2015**, *523*, 196−199.
(78) Penwell, S. B.; Ginsberg, L. D. S.; Noriega, R.; Ginsberg, N. S. Resolving Ultrafast Exciton Migration in Organic Solids at the Nanoscale. *Nat. Mater.* **2017**, *16*, 1136−1142.
(79) Sneyd, A. J.; Beljonne, D.; Rao, A. A New Frontier in Exciton Transport: Transient Delocalization. *J. Phys. Chem. Lett.* **2022**, *13*, 6820−6830.
(80) Balzer, D.; Smolders, T. J. A. M.; Blyth, D.; Hood, S. N.; Kassal, I. Delocalised Kinetic Monte Carlo for Simulating Delocalisation-Enhanced Charge and Exciton Transport in Disordered Materials. *Chem. Sci.* **2021**, *12*, 2276−2285.
(81) Balzer, D.; Kassal, I. Mechanism of Delocalization-Enhanced Exciton Transport in Disordered Organic Semiconductors. *J. Phys. Chem. Lett.* **2023**, *14*, 2155−2162.
(82) Giannini, S.; Peng, W.-T.; Cupellini, L.; Padula, D.; Carof, A.; Blumberger, J. Exciton Transport in Molecular Organic Semiconductors Boosted by Transient Quantum Delocalization. *Nat. Commun.* **2022**, *13*, 2755.

https://doi.org/10.1021/acs.jpclett.3c02286
J. Phys. Chem. Lett. 2023, 14, 10249−10256